TiO_2—Graphene Nanocomposites for Gas-Phase Photocatalytic Degradation of Volatile Aromatic Pollutant: Is TiO_2—Graphene Truly Different from Other TiO_2—Carbon Composite Materials?

Yanhui Zhang,[†,‡] Zi-Rong Tang,[†] Xianzhi Fu,[†,‡] and Yi-Jun Xu[†,‡,*]

[†]College of Chemistry and Chemical Engineering, Fuzhou University, Fuzhou 350108, People's Republic of China, and [‡]State Key Laboratory Breeding Base of Photocatalysis & College of Chemistry and Chemical Engineering, Fuzhou University, Fuzhou 350002, People's Republic of China

ABSTRACT The nanocomposites of TiO_2—graphene (TiO_2—GR) have been prepared *via* a facile hydrothermal reaction of graphene oxide and TiO_2 in an ethanol—water solvent. We show that such a TiO_2—GR nanocomposite exhibits much higher photocatalytic activity and stability than bare TiO_2 toward the gas-phase degradation of benzene, a volatile aromatic pollutant in air. By investigating the effect of different addition ratios of graphene on the photocatalytic activity of TiO_2—GR systematically, we find that the higher weight ratio in TiO_2—GR will decrease the photocatalytic activity. Analogous phenomenon is also observed for the liquid-phase degradation of dyes over TiO_2—GR. In addition, the key features for TiO_2—GR including enhancement of adsorptivity of pollutants, light absorption intensity, electron—hole pairs lifetime, and extended light absorption range have also been found in the composite of TiO_2 and carbon nanotubes (TiO_2—CNT). These strongly manifest that TiO_2—GR is in essence the same as other TiO_2—carbon (carbon nanotubes, fullerenes, and activated carbon) composite materials on enhancement of photocatalytic activity of TiO_2, although graphene by itself has unique structural and electronic properties. Notably, this key fundamental question remains completely unaddressed in a recent report (*ACS Nano* 2010, *4*, 380) regarding liquid-phase degradation of dyes over the TiO_2—GR photocatalyst. Thus, we propose that TiO_2—GR cannot provide truly new insights into the fabrication of TiO_2—carbon composite as high-performance photocatalysts. It is hoped that our work could avert the misleading message to the readership, hence offering a valuable source of reference on fabricating TiO_2—carbon composites for their application as a photocatalyst in the environment cleanup.

KEYWORDS: graphene · TiO_2 · nanocomposite · photocatalysis · volatile aromatic pollutant

Graphene is a rising star on the horizon of materials science and condensed matter physics.[1] This strictly two-dimensional material exhibits outstanding mechanical, thermal, optical, and electrical properties and has indeed spurred immense interest in designing novel graphene-based materials for a variety of technological applications such as nanoelectronics, biosensing, polymer composites, H_2 production and storage, intercalation materials, drug delivery, supercapacitors, and catalysis.[1−12] Titanium dioxide (TiO_2) is well-known and the most investigated functional material in semiconductor photocatalysis.[13−18] It has been widely used in degradation of environmental pollutants in air or water, as well as selective organic transformations to fine chemicals.[13−22] An appropriate integration of graphene and TiO_2 would give rise to a hybrid nanocomposite that combines desirable properties of respective nanoscaled building blocks for specific applications.[23] As a result, the photocatalytic activity of TiO_2 could be improved for target reactions.

It has been shown previously that the composites of TiO_2 and carbon, including activated carbon, carbon nanotubes (CNTs), and fullerenes, are able to exhibit enhanced photocatalytic performance than TiO_2 alone.[24−36] However, some problems still hinder further promotion of efficiency of the present TiO_2—C composites, such as the weakening of light intensity arriving at catalysts' surface and the lack of reproducibility due to the preparation and treatment variation.[24] Graphene, as a "rising star" material and another allotrope of carbon, has many exceptional properties, such as high electron mobility, theoretically high surface area of ~2600 m^2/g, and high transparency.[1−12] Therefore, it seems reasonable to envision that, in comparison with other carbon allotropes, the integration of TiO_2 with graphene

*Address correspondence to yjxu@fzu.edu.cn.

Received for review September 16, 2010 and accepted November 17, 2010.

Published online November 30, 2010. 10.1021/nn1024219

Figure 1. Sample pictures from top to bottom represent the suspensions of GO with different weight ratios dispersed in the ethanol−water solvent, suspensions of P25−GO with different addition ratios of GO before hydrothermal treatment, suspensions of P25−GR after hydrothermal treatment of P25−GO, and the final P25−GR solid product after washing, filtering, and drying process, in which, from left to right, weight addition ratios are 0.2, 0.5, 1, 2, 5, 10, and 30% GR.

could be much more promising to improve the photocatalytic performance of TiO_2.

Most recently, it has been demonstrated that TiO_2−graphene shows an enhancement of photocatalytic activity for degradation of methylene blue in an aqueous solution.[37] The photocatalytic reduction of graphene oxide nanosheets on TiO_2 thin films leads to a nanocomposite photocatalyst of TiO_2−graphene, which exhibits enhanced activity for degradation of bacteria in an aqueous solution.[38] However, in those research works,[37,38] significant and key fundamental issues remain unaddressed completely because the effect of different addition ratios of graphene into the matrix of TiO_2 did not take into account changing of the photocatalytic activity of TiO_2. Thus, questions are naturally raised. Is the TiO_2−graphene composite truly different from other TiO_2−C (activated carbon, fullerene, or carbon nanotube) composites on enhancement of photocatalytic activity of TiO_2? Can the TiO_2−graphene composite as photocatalyst truly provide new insights into the fabrication of TiO_2−carbon composite as high-performance photocatalysts?

Besides the unresolved fundamental issues as mentioned above, there is hitherto no report on applications of TiO_2−graphene nanocomposite to the photocatalytic degradation of volatile organic pollutants (VOCs) in the gas phase. Among VOCs, the monocyclic aromatic benzene commonly occurs in urban ambient air and is of significant concern regarding environmental health because of its toxic, mutagenic, or carcinogenic properties.[39−41] Benzene mainly comes from combustion of liquid fuels in car engines and also from combustion processes in energy production and domestic heating and from such industrial sources as refineries or cookeries. This air pollutant also contributes to the formation of tropospheric ozone. Degradation of toxic benzene into harmless CO_2 by semiconductor-based photocatalysis would present a green and ideal route to eliminate the benzene pollution in air.[25,42]

Herein, we show for the first time that TiO_2−graphene (TiO_2−GR) nanocomposite can be used as a photocatalyst under ambient conditions with much higher activity and stability toward the gas-phase degradation of benzene than the bare TiO_2. The influence of graphene on the photocatalytic activity of TiO_2−GR

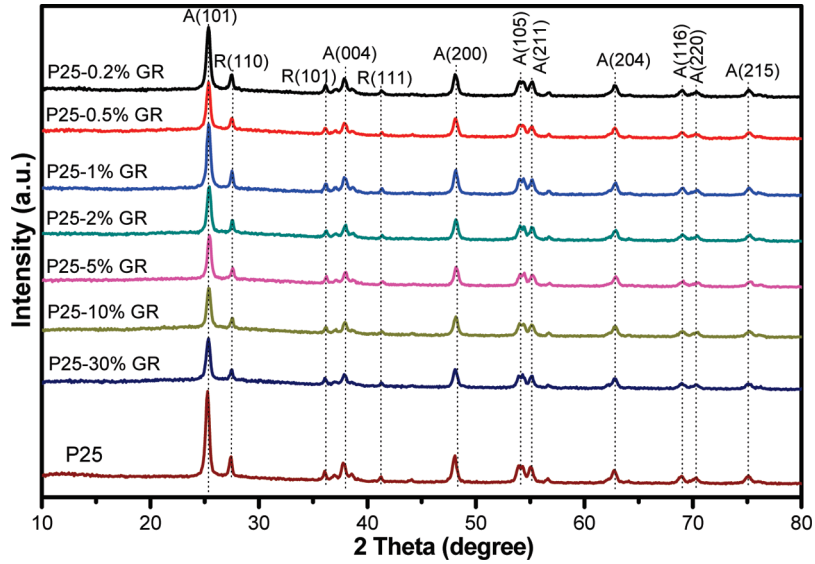

Figure 2. XRD patterns of the P25−GR nanocomposites, in which A is the anatase phase and R is the rutile phase.

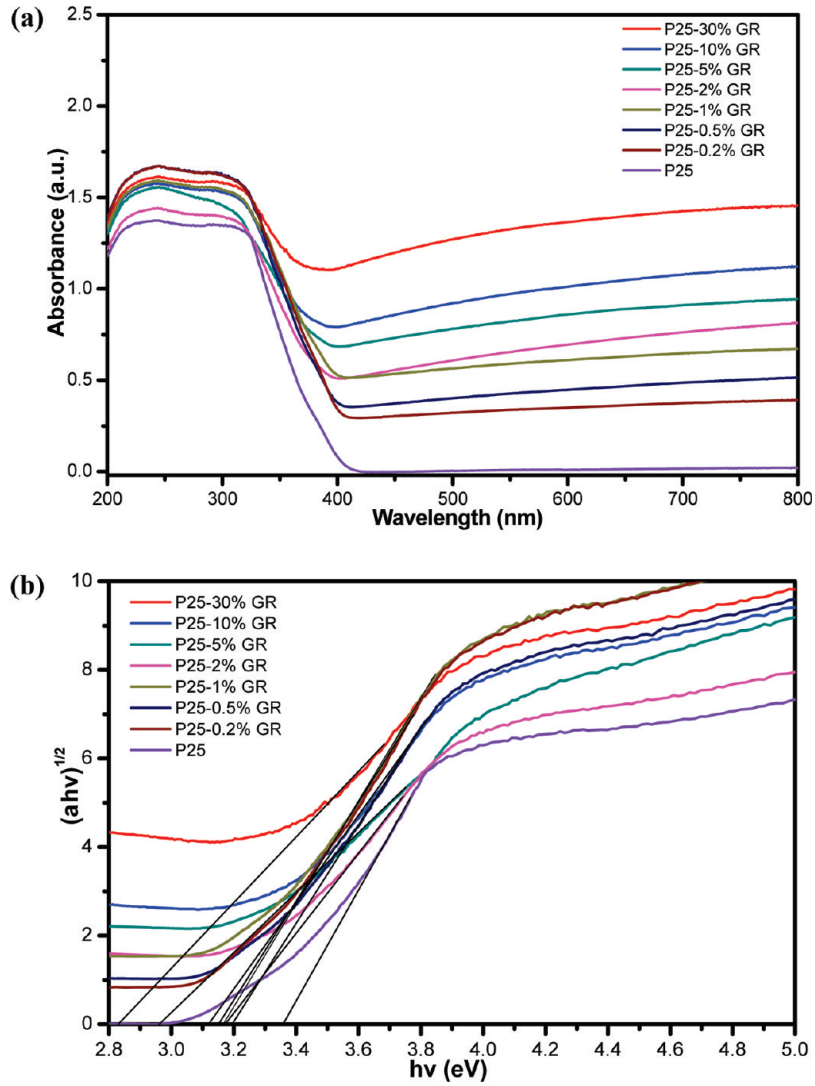

Figure 3. UV−vis diffuse reflectance spectra (DRS) of P25−GR nanocomposites (a), and the plot of transformed Kubelka−Munk function *versus* the energy of light (b).

nanocomposites has been examined systematically by considering different addition ratios of graphene. It is found that the higher addition of graphene in TiO_2−GR nanocomposite leads to a decreased photocatalytic activity. The same phenomenon is also observed in the liquid-phase degradation of dyes over TiO_2−GR nanocomposites. In addition, the key features for TiO_2−GR including the increased adsorptivity of pollutants, enhanced light absorption intensity and light absorption range, and facile charge transportation and separation have also been found previously in the nanocomposite of TiO_2 and carbon nanotubes (TiO_2−CNT). Therefore, more significantly, our present work strongly highlights that TiO_2−graphene is in essence the same as other TiO_2−carbon (carbon nanotubes, fullerenes, and activated carbon) composite materials on enhancement of photocatalytic activity of TiO_2, although graphene by itself has unique structural and electronic properties in comparison with other carbon allotropes. In this regard, it is hoped that our work could avert the misleading message to the readership, hence offering a useful source of reference on fabricating or designing TiO_2−carbon composites for their application as photocatalyst in environment remediation.

RESULTS AND DISCUSSION

A series of nanocomposites of P25 and graphene (GR), denoted as P25−GR, have been obtained by a simple hydrothermal treatment of P25 nanoparticles and graphene oxide (GO) in the solvent of ethanol−water. This treatment process under the solvothermal condition will easily reduce GO to GR while, simultaneously, the particles of P25 are dispersed on the GR sheet.[37,47] Figure 1 displays the sample pictures of suspensions of GO, mixture of P25 and GO before hydrothermal treatment, mixture of P25 and GR after hydrothermal treatment, and the final solid nanocomposite of P25−GR with different weight addition ratios of GR. Clearly, with the increased weight addition of GR, the color of P25−GR product changes from grayish to black. Similar phenomenon is indeed also observed for

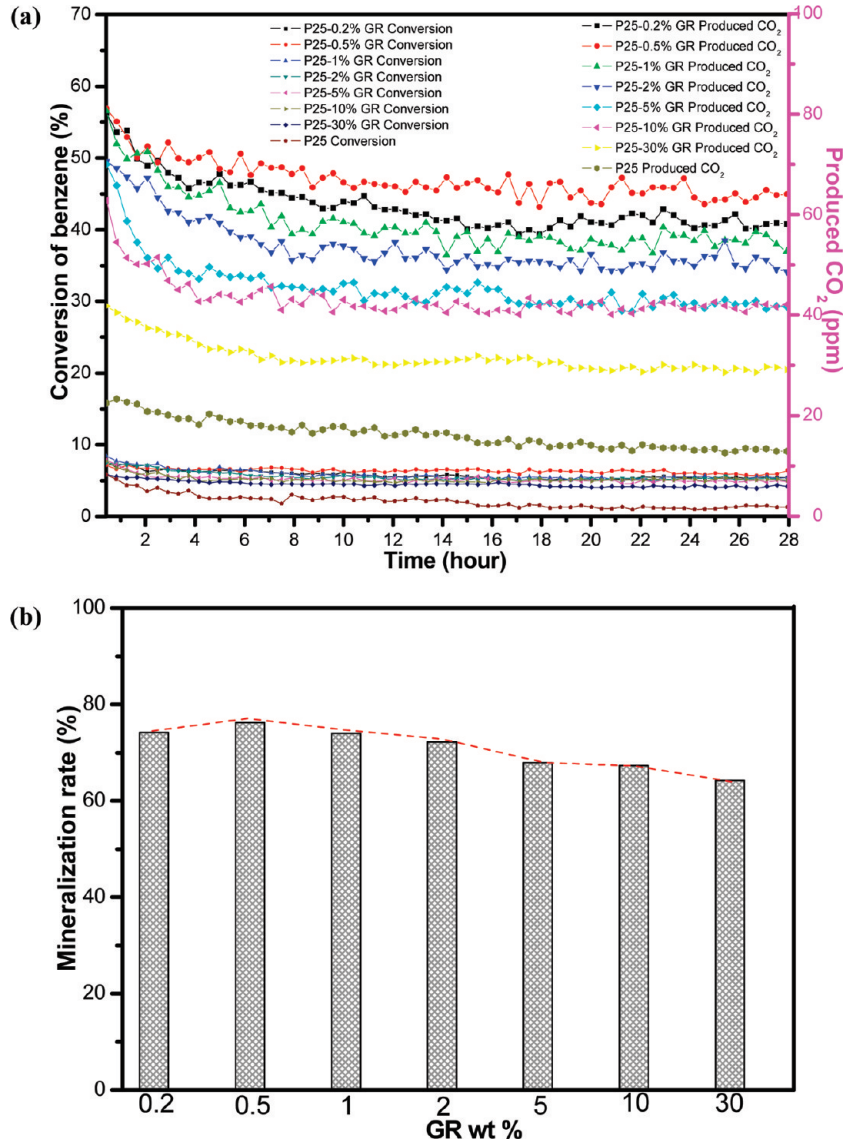

Figure 4. Time-online data for gas-phase photocatalytic degradation of benzene (a), and mineralization ratio (b) over the P25−GR nanocomposites.

other carbon−TiO_2 composite materials, such as the nanocomposite of carbon nanotube and TiO_2 (TiO_2−CNT).[24−27]

The XRD patterns of the as-prepared P25−GR composites are shown in Figure 2. It is obvious that the P25−GR nanocomposites with different weight addition ratios of GR exhibit similar XRD patterns. The peaks at 2θ values of 25.3, 37.8, 48.0, 53.9, 55.1, 62.7, 68.8, 70.3, and 75.0° can be indexed to (101), (004), (200), (105), (211), (204), (116), (220), and (215) crystal planes of anatase TiO_2 in P25, respectively. In addition, characteristic diffraction peaks at 27.4, 36.1, and 41.2° are also observed, which are attributed to the (110), (101), and (111) faces of rutile TiO_2 in P25. Notably, no typical diffraction peaks belonging to the separate GR are observed in the P25−GR nanocomposites. The reason can be ascribed to the fact that the main characteristic peak of GR at 24.5° (Figure S2 in the Supporting Information) might be shielded by the main peak of anatase TiO_2 at 25.4°.[25]

Figure 3a shows the UV−vis diffuse reflectance spectra (DRS) of the P25−GR nanocomposites. The presence of different amounts of GR affects the optical property of light absorption for the P25−GR nanocomposites significantly. The addition of GR induces the increased light absorption intensity in the UV region, as observed in all of the P25−GR nanocomposites with different addition ratios of GR. Meanwhile, in line with previous work regarding using the P25−1% GR nanocomposite for liquid-phase degradation of methylene blue,[37] a red shift to higher wavelength in the absorption edge of P25−GR nanocomposites has also been observed, therefore indicating a narrowing of the band gap of P25. However, it is difficult to determine the value for such a red shift because the background absorption ranging from 400 to 800 nm is increased upon

the incorporation of graphene into the matrix of P25. A plot of the transformed Kubelka−Munk function as a function of energy of light is shown in Figure 3b, by which the roughly estimated band gaps are 2.83, 3.02, 2.96, 3.17, 3.16, 3.19, 3.15, and 3.36 eV corresponding to P25−30% GR, P25−10% GR, P25−5% GR, P25−2% GR, P25−1% GR, P25−0.5% GR, P25−0.2% GR, and bare P25, respectively. This supports the qualitative observation of a red shift in the absorption edge of P25−GR nanocomposites as compared to the bare P25. Analogous band gap narrowing of TiO_2 is also found in the case of TiO_2−CNT composite materials,[24−28] which could be attributed to the chemical bonding between TiO_2 and the specific sites of carbon. In addition, the presence of GR leads to a continuous absorption band in the range of 400−800 nm, which is in agreement with the black color of the samples. The stronger absorption intensity of light for the P25−GR nanocomposites than bare P25 suggests that they could have higher photocatalytic activity for a given reaction. This hypothesis is confirmed by the following gas-phase degradation of benzene over the P25−GR nanocomposites under ambient conditions.

The photocatalytic performance over the P25−GR nanocomposites for gas-phase degradation of benzene has been performed at room temperature and ambient pressure. Blank experiments at the same conditions show that no activity is observed in the absence of catalyst or light irradiation. The controlled blank experiment over the bare GR also shows no photocatalytic activity for degradation of benzene. The adsorption equilibrium in the dark over P25−GR shows that the higher addition amount of GR improves the adsorptivity of benzene (Figure S3), which is also observed in other TiO_2−carbon composites as photocatalyst for degradation of pollutants.[24−29,37] Figure 4 shows the conversion of benzene, the amount of produced CO_2, and the mineralization ratio over the P25−GR photocatalysts and bare P25. It is clear to see from Figure 4a that all of the P25−GR photocatalysts exhibit much higher activity and stability than the reference catalyst of bare P25. The photocatalytic efficiency, based on the benzene conversion rate and produced CO_2 amount, follows the order P25−0.5% GR > P25−0.2% GR > P25−1% GR > P25−2% GR > P25−5% GR > P25−10% GR > P25−30% GR. Namely, the P25−0.5% GR nanocomposite shows the best photocatalytic performance toward the degradation of benzene. Moreover, the mineralization ratio over these P25−GR photocatalysts also shows the same trend, as displayed in Figure 4b. It should be particularly noted that the higher addition ratio of GR will lower the photocatalytic activity of the P25−GR nanocomposite for degradation of benzene. These results suggest a synergistic effect between the GR sheet and TiO_2 nanoparticles. Thus, in order to achieve an optimal photocatalytic performance, it is crucial to control the composition ratio in the nanocomposite of TiO_2−GR. Analogous feature is also observed in the TiO_2−carbon nanotube (TiO_2−CNT) composite materials for the gas-phase degradation of acetone and benzene, in which the addition weight ratio of the CNT for obtaining the maximum photocatalytic activity is generally not higher than 20%.[25,27] The higher addition ratio of GR or CNT into the matrix increases the adsorptivity of pollutants on one hand; however, on the other hand, this also lowers the contact surface of TiO_2 particles with the light irradiation, which would lead to a decreased photocatalytic activity.

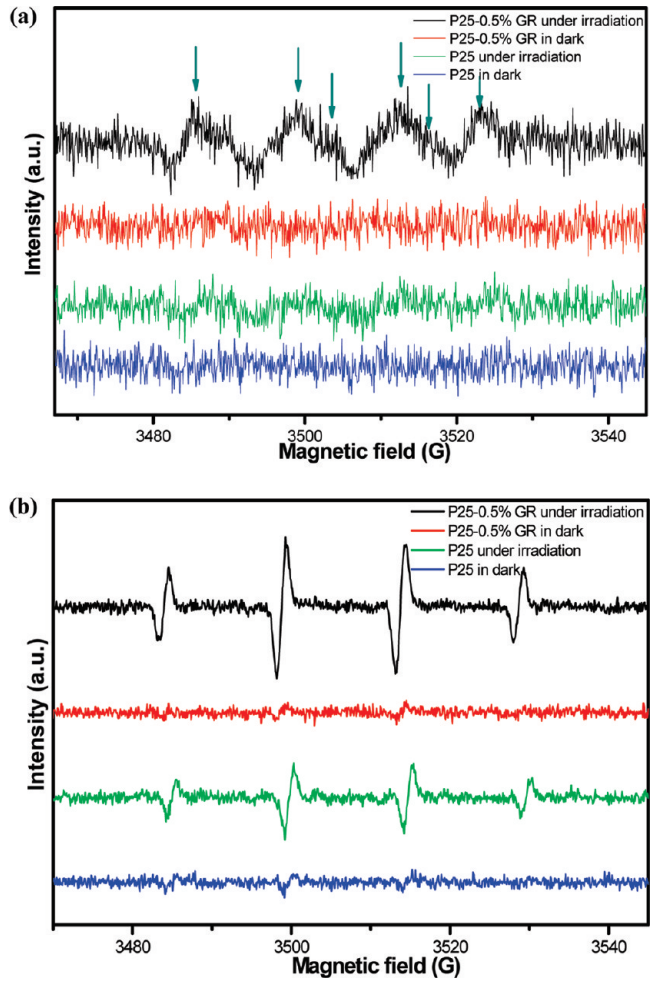

Figure 5. ESR spectra of radical adducts trapped by DMPO in P25 and P25−0.5% GR dispersions: (a) DMPO-$O_2^{-\bullet}$ formed in irradiated methanol dispersions; (b) DMPO-$^{\bullet}$OH formed in irradiated aqueous dispersions.

With regard to the best photocatalyst of P25−0.5% GR, it has a very stable activity toward degradation of benzene in the gas phase because the conversion of benzene is maintained at 6.4%, nearly irrespective of the reaction time. After 10 h of reaction, the produced CO_2 is maintained at an average amount of 67 ppm, which corresponds to an average mineralization ratio of 76.2%. No obvious deactivation is observed over such a P25−0.5% GR nanocomposite in view of the benzene conversion and produced CO_2 amount. However, over the bare P25, it can be clearly found that the

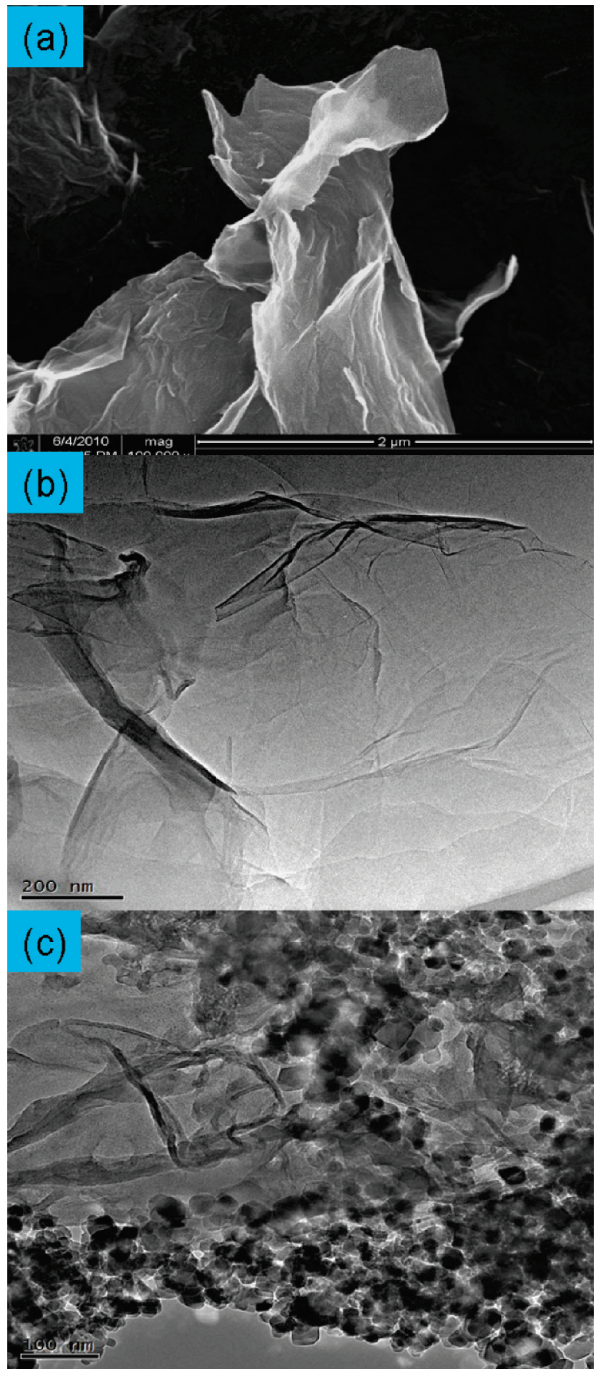

Figure 6. Typical SEM image of GO (a), TEM images of GR (b), and the P25−0.5% GR (c) nanocomposite.

conversion of benzene significantly decreases from 5.8% at the initial stage to 1.2% with time on stream for 28 h. Also, the produced amount of CO_2 decreased to only 12 ppm. This represents that the percentage of decrease of activity over the bare P25 is around 76.9%. The unstable photocatalytic performance of P25 for gas-phase degradation of benzene can be attributed to the blockage of photocatalytic active sites by stable intermediates on the surface of TiO_2 during the reaction,[25,48] thereby leading to the deactivation of bare P25. In this sense, the addition of an appropriate amount of GR is able to enhance the photocatalytic performance of P25 effectively toward the gas-phase degradation of benzene. In addition, it should be mentioned that the extended light absorption band by the addition of GR into the matrix of P25 is not beneficial at all for the gas-phase degradation of benzene under the irridiation of visible light because only the trace conversion of benzene is observed. Similar phenomenon is also found in our previous study regarding the case over the TiO_2−CNT nanocomposites.[25] Therefore, the stable and higher photocatalytic performance over P25−0.5% GR for the degradation of benzene under the irradiation of UV light can be primarily attributed to the three characteristic features associated with P25−0.5% GR composite material. The first two factors are the increased adsorptivity of pollutants and increased light absorption intensity due to the addition of GR into the matrix of P25, as mentioned above. Another key role of GR in the P25−GR nanocomposites is able to trap and shuttle photogenerated electrons,[49] which is similar to CNT in the TiO_2−CNT composite materials.[24−29] For the P25−GR nanocomposite, the excited photogenerated electrons of TiO_2 can transfer from the conduction band to graphene by a percolation mechanism.[50] Furthermore, the two-dimensional planar π-conjugation structure endows graphene with the very excellent conductivity of electrons.[51] These lead to the fact that the presence of graphene in the P25−GR nanocomposite can effectively inhibit the electron−hole pair recombination. Consequently, the lifetime of charge carriers over the photocatalyst is prolonged, which in turn causes the formation of the larger amount of radical species with strong oxidation capability, such as hydroxyl radical and superoxide radical species, for the degradation of pollutant. This hypothesis is faithfully confirmed by the electron spin resonance (ESR) spectra analysis. As shown in Figure 5, the signal of intensity of the formed hydroxyl radical and superoxide radical species in P25−0.5% GR is much stronger than that in the bare P25, thus accounting for a higher stable photocatalytic performance of P25−0.5% GR than the bare P25 toward the degradation of pollutants.

To investigate the effect of hydrothermal treatment time on the photocatalytic activity of the P25−GR nanocomposite, we have synthesized the P25−0.5% GR nanocomposites by the hydrothermal reaction of P25 and GO for 3 and 12 h, respectively, which are used to compare with the P25−0.5% GR nanocomposite by the hydrothermal treatment for 24 h. Figure S4 shows the photocatalytic data for the degradation of benzene over these three P25−GR photocatalysts. It can be concluded that the longer hydrothermal treatment of P25 and GO leads to a P25−GR nanocomposite with a higher photocatalytic activity, which could be due to the increased synergistic interaction (for example, the enhanced chemical bonding) between TiO_2 nanoparticles and the two-dimensional GR sheet. This suggests

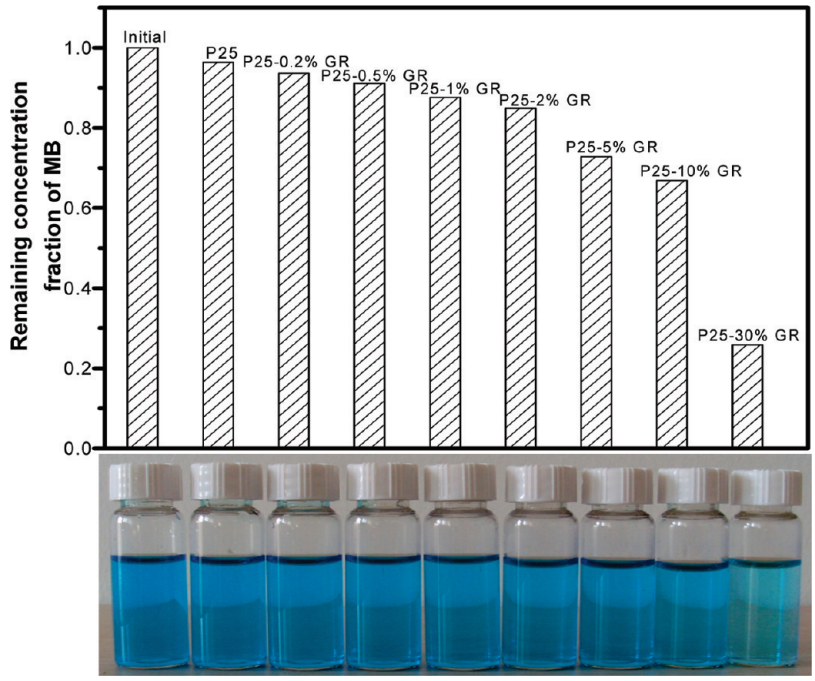

Figure 7. Top: bar plot showing the remaining methylene blue (MB) in solution after reaching the adsorption equilibrium in the dark over the P25−GR nanocomposites. Bottom: pictures of the corresponding MB solution of each sample in the adsorption equilibrium.

that the photocatalytic performance of P25−GR can be further improved by optimizing the detailed synthesis conditions. To obtain the microscopic structure information, we have carried out the transmission electron microscopy (TEM) analysis of the P25−0.5% GR nanocomposite along with the bare GO for comparison, as shown in Figure 6. It is clear that the two-dimensional structure of GR sheets with micrometers-long wrinkles is still retained after the hydrothermal treatment of GO and P25 nanoparticles. In the P25−0.5% GR nanocomposite, the GR sheets are well-decorated by the TiO_2 nanoparticles, which is in line with previous observation on the P25−1% GR nanocomposite for liquid-phase degradation of methylene blue.[37]

Let us give a brief summary of the above results for characterization of the P25−GR photocatalyst and gas-phase degradation of benzene. The addition of a certain amount of graphene into the matrix of TiO_2 can give the P25−GR nanocomposite several excellent characteristics: the increased adsorptivity of pollutants, improved light absorption intensity and extended light absorption range, and enhanced transportation of photogenerated charge carriers. However, these features have been well-observed previously in the composite of TiO_2 and carbon nanotubes (TiO_2−CNT).[24−28] Moreover, similar to the composites of TiO_2−C (CNT or activated carbon or fullerene), we have also found that the higher addition amount of GR is not beneficial to enhance the photocatalytic performance of TiO_2 in comparison to the lower addition amount of GR. Indeed, similar observation can also be found obviously in the liquid-phase degradation of methylene blue (MB) over the P25−GR photocatalysts. Figure 7 displays the sample pictures of the remaining solution of MB after reaching the adsorption equilibrium in the dark over the bare P25 and P25−GR photocatalysts. Similar to the case for degradation of benzene, all of the P25−GR photocatalysts exhibit enhanced adsorptivity of MB as compared to the bare P25, which is also observed in the TiO_2−CNT or TiO_2-activated carbon composites for liquid-phase degradation of dyes.[24−26] The photocatalytic degradation efficiency of MB under both UV light and visible light follows the order P25−5% GR > P25−10% GR > P25−2% GR > P25−1% GR > P25−0.5% GR > P25−0.2% GR > bare P25 > P25−30% GR, as shown in Figure 8. Clearly, when the weight addition ratio of GR is increased to 10%, the activity of P25−10% will be lower than P25−5% GR, although it is higher than bare P25. Further increase of the weight addition ratio of GR will lead to a significant decrease of photocatalytic activity because the P25−30% GR nanocomposite shows lower photocatalytic activity than bare P25 for degradation of MB. Analogous activity trend for photocatalytic degradation of methyl orange (MO), another well-known dye in industrial wastewater, is also observed over the P25−GR nanocomposites (Figures S5 and S6). The greater enhancement of photocatalytic activity under the irradiation of visible light for liquid-phase degradation of dyes over P25−GR than the case for gas-phase degradation of benzene as mentioned above suggests that benzene is more difficult for photocatalytic degradation, which could be due to its more stable and inert chemical structure. Thus far, on

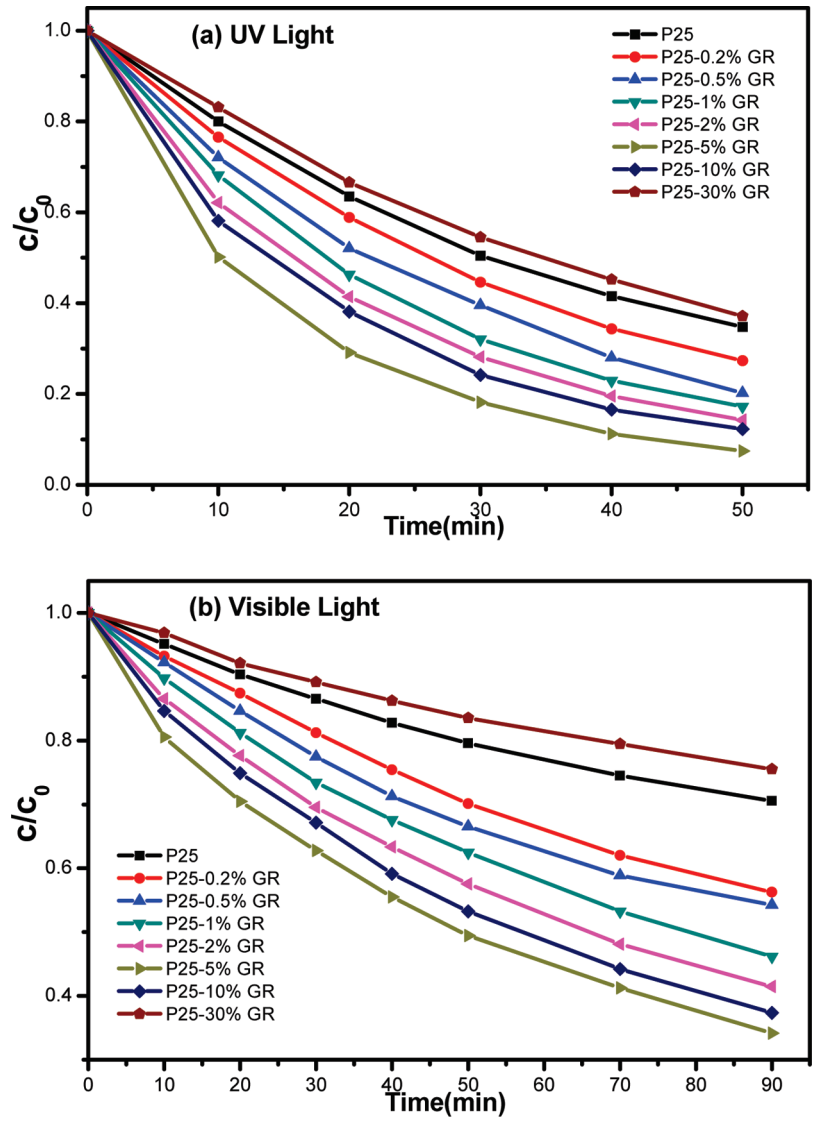

Figure 8. Liquid-phase photocatalytic degradation of methylene blue (MB) under the irradiation of (a) UV light and (b) visible light (λ > 400 nm) over the P25−GR nanocomposites.

the basis of the results for gas-phase degradation of benzene and liquid-phase degradation of dyes, we argue that the nanocomposites of TiO_2−GR as photocatalyst are the same in essence as that other TiO_2−carbon (carbon nanotube, activated carbon, and fullerene) composite materials on enhancement of photocatalytic activity of semiconductor TiO_2, although graphene by itself has unique structural and electronic properties in comparison with other carbon allotropes. In addition, a schematic illustration model for the photocatalytic gas-phase and liquid-phase degradation of organic pollutants including benzene and dyes is proposed in Figure 9, which is also similar to the case over the photocatalyst of TiO_2−CNT nanocomposites.[25]

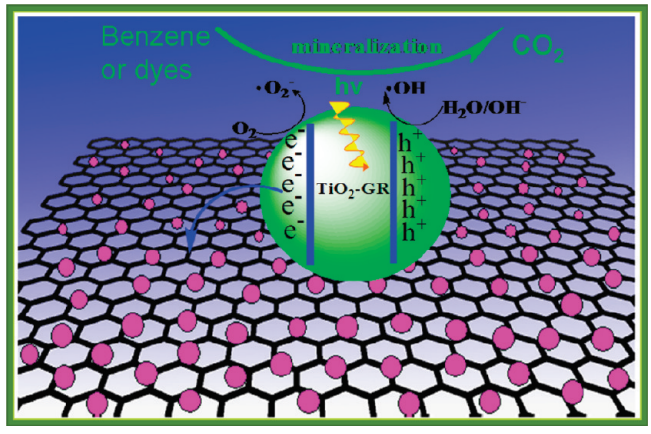

Figure 9. Proposed schematic illustration showing the reaction mechanism for photocatalytic degradation of organic pollutants (benzene or dyes) over the P25−GR nanocomposites in which pink spheres and black sheet represent TiO_2 nanoparticles and GR, respectively.

In a recent study, Zhang and co-workers prepared the photocatalyst of P25−1% GR for the liquid-phase degradation of methylene blue (MB).[37] For comparison, a photocatalyst of P25−1% CNT was also prepared. Under the irradiation of both UV light and visible light, they observed a higher degradation efficiency of MB by only *ca.* 15% over P25−1% GR than P25−1% CNT.

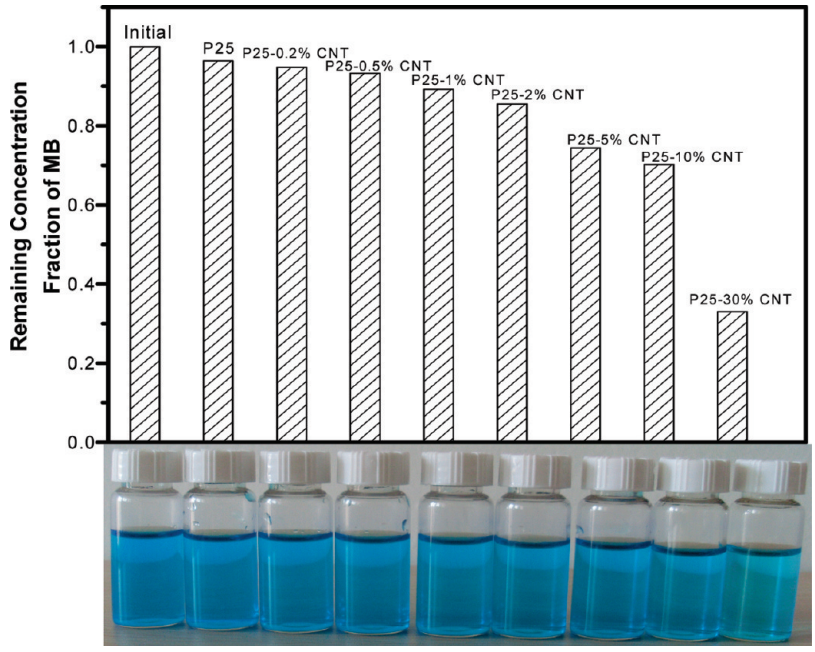

Figure 10. Top: bar plot showing the remaining methylene blue (MB) in solution after reaching the adsorption equilibrium in the dark over the P25−CNT nanocomposites. Bottom: pictures of the corresponding MB solution of each sample in the adsorption equilibrium.

Accordingly, they claimed that TiO_2−GR nanocomposites could provide new insights in the fabrication of TiO_2−carbon composites as high-performance photocatalysts. In fact, the conclusion based on such an observation is not reasonable, because, without investigating the different weight addition ratios of GR or CNT into the matrix of TiO_2 particles, a reasonable comparison of photocatalytic activity between P25−GR and P25−CNT cannot be made reasonably; in other words, it still remains unknown whether GR is truly different from other carbon allotropes on enhancement of photocatalytic activity of TiO_2. In addition, it should be reiterated that the key features observed in the TiO_2−GR composites as reported in the Zhang *et al.*'s work have been indeed observed previously in the composites of TiO_2−CNT,[24−29] namely, the increased adsorptivity of pollutants, enhanced light absorption intensity and light absorption range, and boosted transportation and separation of photogenerated charge carriers.

To better understand this standpoint, using the similar synthesis condition to that in Zhang *et al.*'s work, we have prepared a series of P25−CNT nanocomposites with different addition ratios of CNT and studied their photocatalytic performance for degradation of MB. The data are shown in Figures 10 and 11. Similar to the P25−GR photocatalysts, the higher addition of CNT increases the adsorptivity of MB after reaching the adsorption equilibrium in the dark over P25−CNT. Second, regarding the degradation of MB over P25−CNT under the irradiation of both UV light and visible light, the activity trend is the same as that over the P25−GR photocatalysts, that is, P25−5% CNT > P25−10% CNT > P25−2% CNT > P25−1% CNT > P25−0.5% CNT > P25−0.2% CNT > bare P25 > P25−30% CNT, although the P25-GR nanocomposites exhibit slightly higher activity for degradation of MB than their P25−CNT counterparts. Similar to P25−GR, the extended light absorption range and increased light absorption intensity are also observed for the P25−CNT nanocomposites (Figure S7). Furthermore, the efficient charge transportation and separation have also been well-reported regarding photocatalytic degradation of pollutants over the TiO_2−CNT composites.[24−29,52] Therefore, all of these strongly suggest that GR is in essence the same as CNT on enhancement of photocatalytic performance of TiO_2.

CONCLUSIONS

In summary, we have prepared the nanocomposites of TiO_2−GR with different weight addition ratios of GR by a facile hydrothermal treatment of GO and TiO_2 nanoparticles in a solvent of ethanol−water. It has been showed that the TiO_2−GR nanocomposites can be used as photocatalyst under ambient conditions toward the gas-phase degradation of benzene, a volatile organic pollutant in air. The results show that the TiO_2−GR nanocomposite is able to exhibit much higher stability and activity than that of the bare TiO_2. The influence of GR on the photocatalytic activity of TiO_2−GR nanocomposites has been examined systematically by considering the different weight addition ratios of graphene. It is found that the higher addition of graphene in TiO_2−GR leads to a decreased photocatalytic activity. The same phenomenon is also observed in the liquid-phase degradation of dyes over TiO_2−GR photocatalysts. All of these features have also been

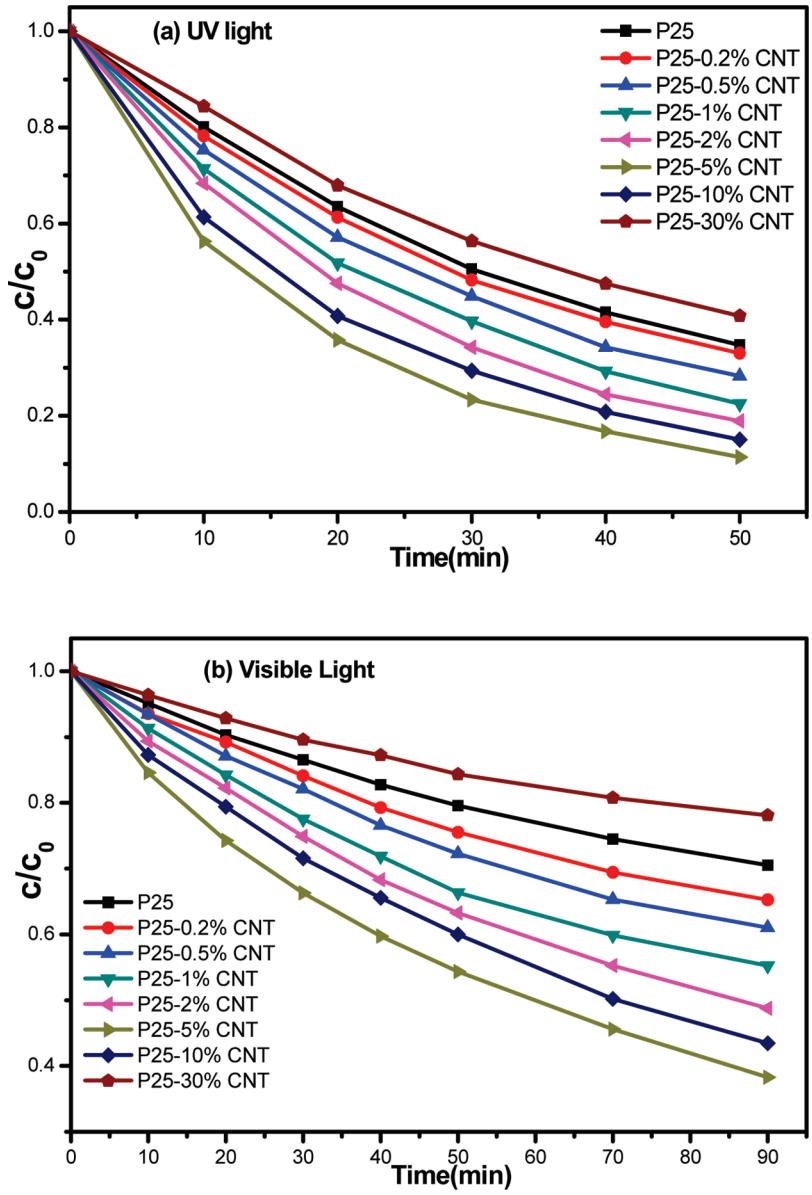

Figure 11. Liquid-phase photocatalytic degradation of methylene blue (MB) under the irradiation of (a) UV light and (b) visible light ($\lambda > 400$ nm) over the P25−CNT nanocomposites.

found in other TiO_2−C composites as photocatalyst, for example, TiO_2−CNT composites. Thus, our present work significantly suggests that TiO_2−GR is in essence the same as other TiO_2−carbon (carbon nanotubes, fullerenes, and activated carbon) composite materials on enhancement of photocatalytic activity of TiO_2, although graphene by itself has unique structural and electronic properties in comparison with other carbon allotropes.

It is hoped that our current work could avert the misleading message to the readership,[37] hence offering a useful source of reference on fabricating or designing TiO_2−carbon composites for their application as photocatalyst in environment remediation.

METHODS

Catalyst Preparation. First, graphene oxide (GO) was synthesized by the modified Hummers' method.[43−46] The detailed synthesis procedures are shown in the Supporting Information. Titanium dioxide (TiO_2) nanopowder is the commercial P25 (supplied from Degussa Co., Ltd., Germany). To synthesize the P25−graphene (P25-GR) nanocomposites with different addition ratios of graphene, a simple hydrothermal method using methanol−water as solvent was used as the following (Scheme 1).[37,47] Under such a solvothermal condition, the solvent of ethanol−water has the strong power to reduce GO to GR.[47]

GO was ultrasonicated in a 60 mL of deionized water and 30 mL of anhydrous ethanol solution to disperse it well; after that, 0.6 g of P25 was added to the calculated amount of the above GO solution to prepare 0.2, 0.5, 1, 2, 5, 10, and 30 wt % GR−P25 nanocomposite catalysts with different weight addition ratios of GR in the nanocomposites of P25−GR. The mixing solution was aged with vigorous stirring for 2 h to obtain a homogeneous sus-

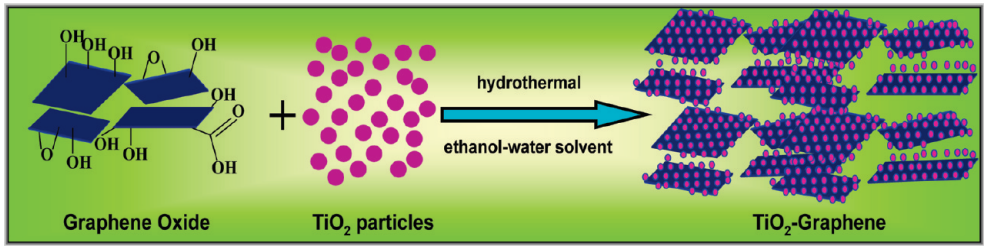

Scheme 1. Flow chart for preparation of P25−GR nanocomposites by a hydrothermal treatment in the solvent of ethanol−water.

pension. Then, this suspension was transferred to a 100 mL Teflon-sealed autoclave and maintained at 120 °C for 24 h. By this hydrothermal treatment, the reduction of GO to GR and the deposition of TiO_2 onto the GR sheet can be simultaneously achieved.[37,47] The resulting composite was recovered by filtration, washed by water, and fully dried at 60 °C in oven to get the final P25−GR nanocomposite with different weight addition ratios of GR.

Catalyst Characterization. The X-ray diffraction (XRD) patterns of the samples were collected on a Bruker D8 Advance X-ray diffractometer with Cu Kα radiation. The accelerating voltage and the applied current were 40 kV and 40 mA, respectively. The optical properties of the samples were analyzed by UV−vis diffuse reflectance spectroscopy (UV−vis DRS) using a UV−vis spectrophotometer (Cary-500, Varian Co.), in which $BaSO_4$ was used as the background. The morphology of the samples was determined by a field emission scanning electron microscopy (FSEM) on a FEI Nova NANOSEM 230 spectrophotometer. Transmission electron microscopy (TEM) images were collected by using a JEOL model JEM 2010 EX microscope at an accelerating voltage of 200 kV. Electron spin resonance (ESR) spectra were measured using a Bruker A300 EPR electron paramagnetic resonance spectrometer equipped with a quanta-Ray Nd:YAG laser system as their radiation light source (λ = 266 nm). The settings were the center field at 3480.00 G, microwave frequency at 9.83 GHz, and power at 6.35 mW.

Catalyst Activity. The photocatalytic gas-phase degradation of benzene was performed in a tubular vessel microreactor operating in a continuous flow mode.[25] The catalyst (0.3 g, 50−70 mesh) was loaded in the reactor surrounded by four 4 W UV lamps with a wavelength centered at 254 nm (Philips, TUV 4W/G4 T5) as the light resource. A bubbler that contained benzene was immersed in an ice−water bath, and benzene (about 250 ppm) bubbled with oxygen from the bubbler was fed to 0.3 g of catalyst at a total flow rate of 20 mL/min. All of the photocatalytic experiments were carried out only after the equilibrium absorption of benzene was achieved. The reaction temperature was controlled at 27 ± 1 °C by an air-cooling system. Simultaneous determination of benzene and CO_2 concentrations was performed with an online gas chromatograph (HP6890) equipped with a flame ionization detector (FID) and a thermal conductivity detector (TCD). Conversion of benzene and mineralization of benzene were defined as the following:

$$\%\text{conversion} = [(C_0 - C)/C_0] \times 100$$

$$\%\text{mineralization} = [(CO_2)_{\text{produced}}/6(\text{benzene})_{\text{converted}}] \times 100$$

where C_0 is the initial concentration of benzene and C is the concentration of benzene after photocatalytic reaction.

The liquid-phase photodegradation of dyes (methylene blue and methyl orange) was carried out in a quartz tube under the irradiation of UV light and visible light, respectively. In a typical process for degradation of dyes under the UV irradiation, a 20 mg portion of catalyst was suspended in 160 mL of 10 ppm dyes solution. Before irradiation, the suspensions were stirred in the dark for 4 h to ensure the establishment of adsorption−desorption equilibrium. Under ambient conditions and stirring, the quartz tube was exposed to the UV irradiation produced by a 500W Xe arc lamp equipped with a band-pass light filter (365 ± 15 nm). A 3 mL sample solution was taken at a certain time interval during the experiment and centrifuged to remove the catalyst completely. The solution was analyzed on a Varian UV−vis spectrophotometer (Cary-50, Varian Co.). The percentage of degradation is reported as C/C_0. Here, C is the absorption of dyes solution at each irradiated time interval of the main peak of the adsorption spectrum, while C_0 is the absorption of the initial concentration when the adsorption−desorption equilibrium is reached. For the visible light photocatalytic degradation of dyes, a UV cutoff filter (λ > 400 nm) was used while the other experimental conditions are the same as that of the above-mentioned degradation of dyes under the UV light irradiation.

Acknowledgment. The support by the National Natural Science Foundation of China (20903022, 20903023), the Award Program for Minjiang Scholar Professorship, Program for Changjiang Scholars and Innovative Research Team in Universities (PCSIRT0818), 973 Program (2007CB613306), and Program for Returned High-Level Overseas Chinese Scholars of Fujian province is gratefully acknowledged. We also cordially thank the valuable comments of the reviewers to improve the quality of our research work. Y.-J. Xu would like to dedicate this work to his newborn baby.

Supporting Information Available: Experimental details for synthesis of graphene oxide, XRD patterns of graphene oxide and graphene, bar plot showing the increased adsorptivity of benzene over P25−GR, time-online data for degradation of benzene over P25−0.5% GR by a hydrothermal treatment for different time, degradation of methyl orange over P25−GR nanocomposites, and the UV−vis DRS data for P25-CNT nanocomposites. This material is available free of charge *via* the Internet at http://pubs.acs.org.

REFERENCES AND NOTES

1. Geim, A. K.; Novoselov, K. S. The Rise of Graphene. *Nat. Mater.* **2007**, *6*, 183–191.
2. Geim, A. K. Graphene: Status and Prospects. *Science* **2009**, *324*, 1530–1534.
3. Allen, M. J.; Tung, V. C.; Kaner, R. B. Honeycomb Carbon: A Review of Graphene. *Chem. Rev.* **2010**, *110*, 132–145.
4. Bunch, J. S.; van der Zande, A. M.; Verbridge, S. S.; Frank, I. W.; Tanenbaum, D. M.; Parpia, J. M.; Craighead, H. G.; McEuen, P. L. Electronmechanical Resonators from Graphene Sheets. *Science* **2007**, *315*, 490–493.
5. Stoller, M. D.; Park, S. J.; Zhu, Y. W.; An, J. H.; Ruoff, R. S. Graphene-Based Ultracapacitors. *Nano Lett.* **2008**, *8*, 3498–3502.
6. Guo, S.; Dong, S.; Wang, E. Three-Dimensional Pt-on-Pd Bimetallic Nanodendrites Supported on Graphene Nanosheet: Facile Synthesis and Used as an Advanced Nanoelectrocatalyst for Methanol Oxidation. *ACS Nano* **2010**, *4*, 547–555.
7. Chen, S.; Zhu, J.; Wu, X.; Han, Q.; Wang, X. Graphene Oxide−MnO_2 Nanocomposites for Supercapacitors. *ACS Nano* **2010**, *4*, 2822–2830.
8. Stankovich, S.; Dikin, D. A.; Dommett, G. H. B.; Kohlhaas, K. M.; Zimney, E. J.; Stach, E. A.; Piner, R. D.; Nguyen, S. T.; Ruoff, R. S. Graphene-Based Composite Materials. *Nature* **2006**, *442*, 282–286.

9. Seger, B.; Kamat, P. V. Electrocatalytically Active Graphene−Platinum Nanocomposites. Role of 2D Carbon Support in PEM Fuel Cells. *J. Phys. Chem. C* **2009**, *113*, 7990–7995.
10. Li, X. L.; Wang, X. R.; Zhang, L.; Lee, S. W.; Dai, H. J. Chemically Derived, Ultrasmooth Graphene Nanoribbon Semiconductors. *Science* **2008**, *319*, 1229–1232.
11. Park, N.; Hong, S.; Kim, G.; Jhi, S. H. Computational Study of Hydrogen Storage Characteristics of Covalent-Bonded Graphenes. *J. Am. Chem. Soc.* **2007**, *129*, 8999–9003.
12. Park, S.; Lee, K. S.; Bozoklu, G.; Cai, W.; Nguyen, S. T.; Ruoff, R. S. Graphene Oxide Papers Modified by Divalent Ions-Enhancing Mechanical Properties *via* Chemical Cross-Linking. *ACS Nano* **2008**, *2*, 572–578.
13. Hoffmann, M. R.; Martin, S. T.; Choi, W.; Bahnemann, D. W. Environmental Applications of Semiconductor Photocatalysis. *Chem. Rev.* **1995**, *95*, 69–96.
14. Fox, M. A.; Dulay, M. T. Heterogenous Photocatalysis. *Chem. Rev.* **1993**, *93*, 341–357.
15. Kamat, P. V. Photochemistry on Nonreactive and Reactive (Semiconductor) Surfaces. *Chem. Rev.* **1993**, *93*, 267–300.
16. Linsebigler, A. L.; Lu, G. Q.; Yates, J. T. Photocatalysis on TiO_2 Surface: Principles, Mechanisms, and Selected Results. *Chem. Rev.* **1995**, *95*, 735–758.
17. Carp, O.; Huisman, C. L.; Reller, A. Photoinduced Reactivity of Titanium Dioxide. *Prog. Solid State Chem.* **2004**, *32*, 33–177.
18. Gaya, U. I.; Abdullah, A. H. Heterogeneous Photocatalytic Degradation of Organic Contaminants over Titanium Dioxide: A Review of Fundamentals, Progress and Problems. *J. Photochem. Photobiol., C* **2008**, *9*, 1–12.
19. Maldotti, A.; Molinari, A.; Amadelli, R. Photocatalysis with Organized Systems for the Oxofunctionalization of Hydrocarbons by O_2. *Chem. Rev.* **2002**, *102*, 3811–3836.
20. Zhang, M.; Wang, Q.; Chen, C. ; Zang, L.; Ma, W.; Zhao, J. Oxygen Atom Transfer in the Photocatalytic Oxidation of Alcohols by TiO_2: Oxygen Isotope Studies. *Angew. Chem., Int. Ed.* **2009**, *48*, 6081–6084.
21. Palmisano, G.; Augugliaro, V.; Pagliaro, M.; Palmisano, L. Photocatalysis: A Promising Route for 21st Century Organic Chemistry. *Chem. Commun.* **2007**, 3425–3437.
22. Shiraishi, Y.; Hirai, T. Selective Organic Transformations on Titanium Oxide-Based Photocatalysts. *J. Photochem. Photobiol., C* **2008**, *9*, 157–170.
23. Kamat, P. V. Graphene-Based Nanoarchitectures. Anchoring Semiconductor and Metal Nanoparticles on a Two-Dimensional Carbon Support. *J. Phys. Chem. Lett.* **2010**, *1*, 520–527.
24. Woan, K.; Pyrgiotakis, G.; Sigmund, W. Photocatalytic Carbon-Nanotube-TiO_2 Composites. *Adv. Mater.* **2009**, *21*, 2233–2239.
25. Xu, Y. J.; Zhuang, Y. B.; Fu, X. Z. New Insight for Enhanced Photocatalytic Activity of TiO_2 by Doping Carbon Nanotubes: A Case Study on Degradation of Benzene and Methyl Orange. *J. Phys. Chem. C* **2010**, *114*, 2669–2676.
26. Yu, Y.; Yu, J. C.; Chan, C. Y.; Che, Y. K.; Zhao, J. C.; Ding, L.; Ge, W. K.; Wong, P. K. Enhancement of Adsorption and Photocatalytic Activity of TiO_2 by Using Carbon Nanotubes for the Treatment of Azo Dye. *Appl. Catal., B* **2005**, *61*, 1–11.
27. Yu, Y.; Yu, J. C.; Yu, J. G.; Kwok, Y. C.; Che, Y. K.; Zhao, J. C.; Ding, L.; Ge, W. K.; Wong, P. K. Enhancement of Photocatalytic Activity of Mesoporous TiO_2 by Using Carbon Nanotubes. *Appl. Catal., A* **2005**, *289*, 186–196.
28. Yao, Y.; Li, G. H.; Ciston, S.; Lueptow, R. M.; Gray, K. A. Photoreactive TiO_2/Carbon Nanotube Composites: Synthesis and Reactivity. *Environ. Sci. Technol.* **2008**, *42*, 4952–4957.
29. Wang, W.; Serp, P.; Kalck, P.; Faria, J. L. Photocatalytic Degradation of Phenol on MWNT and Titania Composite Catalysts Prepared by a Modified Sol−Gel Method. *Appl. Catal., B* **2005**, *56*, 305–312.
30. Tryba, B.; Morawski, A. W.; Inagaki, M. Application of TiO_2-Mounted Activated Carbon to the Removal of Phenol from Water. *Appl. Catal., B* **2003**, *41*, 427–433.
31. Wang, W. D.; Silva, C. G.; Faria, J. L. Photocatalytic Degradation of Chromotrope 2R Using Nanocrystalline TiO_2/Activated-Carbon Composite Catalysts. *Appl. Catal., B* **2007**, *70*, 470–478.
32. Li, Y. J.; Li, X. D.; Li, J. W.; Yin, J. Photocatalytic Degradation of Methyl Orange by TiO_2-Coated Activated Carbon and Kinetic Study. *Water Res.* **2006**, *40*, 1119–1126.
33. Oh, W. C.; Jung, A. R.; Ko, W. B. Preparation of Fullerene/TiO_2 Composite and Its Photocatalytic Effect. *J. Ind. Eng. Chem.* **2007**, *13*, 1208–1214.
34. Lin, J.; Zong, R. L.; Zhou, M.; Zhu, Y. F. Photoelectric Catalytic Degradation of Methylene Blue by C_{60}-Modified TiO_2 Nanotube Array. *Appl. Catal., B* **2009**, *89*, 425–431.
35. Long, Y.; Lu, Y.; Huang, Y.; Peng, Y.; Lu, Y.; Kang, S. Z.; Mu, J. Effect of C_{60} on the Photocatalytic Activity of TiO_2 Nanorods. *J. Phys. Chem. C* **2009**, *113*, 13899–13905.
36. Fu, H.; Xu, T.; Zhu, S.; Zhu, Y. Photocorrosion Inhibition and Enhancement of Photocatalytic Activity for ZnO *via* Hybridization with C_{60}. *Environ. Sci. Technol.* **2008**, *42*, 8064–8069.
37. Zhang, H.; Lv, X. J.; Li, Y. M.; Wang, Y.; Li, J. H. P25-Graphene Composite as a High Performance Photocatalyst. *ACS Nano* **2010**, *4*, 380–386.
38. Akhavan, O.; Ghaderi, E. Photocatalytic Reduction of Graphene Oxide Nanosheets on TiO_2 Thin Film for Photoinactivation of Bacteria in Solar Light Irradiation. *J. Phys. Chem. C* **2009**, *113*, 20214–20220.
39. Lan, Q.; Zhang, L.; Li, G.; Vermeulen, R. V.; Weinberg, R. S.; Dosemeci, M.; Rappaport, S. M.; Shen, M.; Alter, B. P.; Wu, Y.; *et al.* Hematotoxicity in Workers Exposed to Low Levels of Benzene. *Science* **2004**, *306*, 1774–1776.
40. Priority Pollutants. Code of Federal Regulations, Title 40; U.S. Environmental Protection Agengy, U.S. Government Printing Office: Washington, D.C., 1996; Chapter 1, Part 423, App.A.
41. Wilkinson, C. F. Being More Realistic about Chemical Carcinogenesis. *Environ. Sci. Technol.* **1987**, *21*, 843–847.
42. Fu, X. Z.; Zeltner, W. A.; Anderson, M. A. The Gas-Phase Photocatalytic Mineralization of Benzene on Porous Titania-Based Catalysts. *Appl. Catal., B* **1995**, *6*, 209–224.
43. Hummers, W. S.; Offeman, R. E. Preparation of Graphitic Oxide. *J. Am. Chem. Soc.* **1958**, *80*, 1339.
44. Kovtyukhova, N. I.; Ollivier, P. J.; Martin, B. R.; Mallouk, T. E.; Chizhik, S. A.; Buzaneva, E. V.; Gorchinskiy, A. D. Layer-by-Layer Assembly of Ultrathin Composite Films from Micron-Sized Graphite Oxide Sheets and Polycations. *Chem. Mater.* **1999**, *11*, 771–778.
45. Pan, D. Y.; Wang, S.; Zhao, B.; Wu, M. H.; Zhang, H. J.; Wang, Y.; Jiao, Z. Li Storage Properties of Disordered Graphene Nanosheets. *Chem. Mater.* **2009**, *21*, 3136–3142.
46. Cote, L. J.; Kim, F.; Huang, J. X. Langmuir−Blodgett Assembly of Graphite Oxide Single Layers. *J. Am. Chem. Soc.* **2009**, *131*, 1043–1049.
47. Nethravathi, C.; Rajamathi, M. Chemically Modified Graphene Sheets Produced by the Solvothermal Reduction of Colloidal Dispersions of Graphite Oxide. *Carbon* **2008**, *46*, 1994–1998.
48. Hou, Y.; Wang, X.; Wu, L.; Ding, Z.; Fu, X. Efficient Decomposition of Benzene over a β-Ga_2O_3 Photocatalyst under Ambient Conditions. *Environ. Sci. Technol.* **2006**, *40*, 5799–5803.
49. Willams, G.; Seger, B.; Kamat, P. V. TiO_2-Graphene Nanocomposites. UV-Assisted Photocatalytic Reduction of Graphene Oxide. *ACS Nano* **2008**, *2*, 1487–1491.
50. Wang, X.; Zhi, L. J.; Müllen, K. Conductive Graphene Electrodes for Dye-Sensitized Solar Cells. *Nano Lett.* **2008**, *8*, 323–327.
51. Novoselov, K. S.; Geim, A. K.; Morozov, S. V.; Jiang, D.; Zhang, Y.; Dubonos, S. V.; Grigorieva, I. V.; Firsov, A. A. Electric Field Effect in Atomically Thin Carbon Films. *Science* **2004**, *306*, 666–669.
52. Kongkanand, A.; Kamat, P. V. Electron Storage in Single Wall Carbon Nanotubes. Fermi Level Equilibration in Semiconductor−SWCNT Suspensions. *ACS Nano* **2007**, *1*, 13–21.